LETTERS
PUBLISHED ONLINE: 6 FEBRUARY 2011 | DOI: 10.1038/NGEO1078
nature geoscience

Weakening of the equatorial Atlantic cold tongue over the past six decades

Hiroki Tokinaga[1]* and Shang-Ping Xie[1,2]

Seasonal and interannual variations of the equatorial cold tongue are defining features of the tropical Atlantic Ocean, with significant climatic[1–3] and biogeochemical[4] effects. However, its long-term changes are poorly understood owing to biases in observations and climate models[5]. Here we use a suite of bias-corrected observations, and find that cold-tongue variability has weakened during the past six decades. We find that sea surface temperature has increased across the basin, with a local enhancement over the eastern equatorial Atlantic. This warming pattern of the sea surface is most pronounced during boreal summer, reducing the annual cycle through a positive ocean–atmosphere feedback. Specifically, the eastward-intensified warming leads to enhanced atmospheric convection in the equatorial eastern Atlantic region, as well as to less vigorous trade winds. These in turn deepen the thermocline in the east, and reinforce the sea surface warming pattern. The flattened thermocline and reduced thermocline feedback weaken interannual variability of equatorial sea surface temperatures and Guinea coast precipitation associated with the Atlantic Niño. We suggest that the observed changes could be associated with cooling by anthropogenic aerosols, an effect that is stronger in the Northern than in the Southern Hemisphere. If the aerosol emissions decrease in the next decades, the tropical Atlantic may experience yet another shift as the greenhouse gas forcing increases.

Regional patterns of sea surface temperature (SST) change have received much attention lately because of their importance for local rainfall and remote climate effects[6,7]. Over the Pacific Ocean, the Coupled Model Intercomparison Project phase 3 (CMIP3) models predict an equatorial-enhanced warming[8], which anchors an equatorial band of precipitation increase with potential effects on tropical cyclones[6]. Observed changes over the Pacific, however, are still controversial, depending on the data set and study period[9]. In the tropical Indian Ocean, patterns of recent SST and sea-level changes are under active debate[10,11]. Whereas coral records[12] and coupled general circulation models[11] (GCMs) indicate a positive Indian Ocean dipole-like change in SST and sea level, ocean GCM hindcasts forced by atmospheric reanalyses indicate an opposite change over the past half-century[10]. There has been little discussion about tropical Atlantic change, partly because of large biases in coupled GCMs, most notably their poor simulation of the equatorial cold tongue and trade winds[5]. Equatorial Atlantic SST influences climate over the ocean and surrounding continents, as illustrated by the Atlantic Niño with increased (decreased) precipitation over the Guinea coast and the equatorial Amazon (the African Sahel)[1–3] for a warm SST event.

To identify patterns of recent climate change over the tropical Atlantic, we use a suite of historical observations with careful quality controls (see Methods). There are three main ship lanes

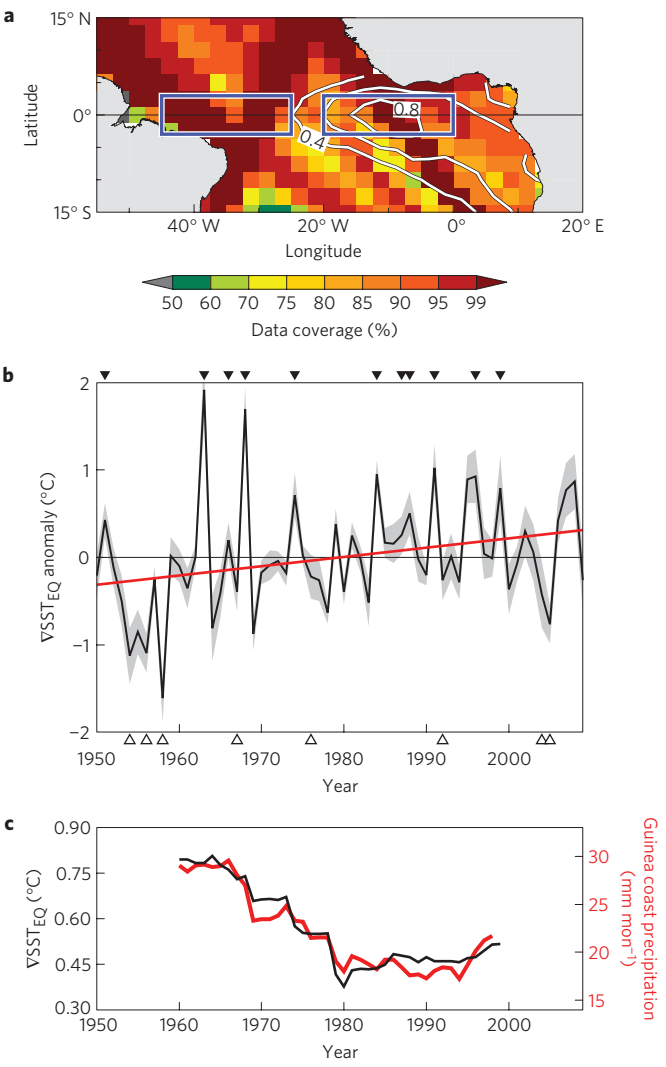

Figure 1 | Weakening of the equatorial Atlantic cold tongue and reduced Atlantic Niño variability. a, Per cent of months with at least one ship observation of SST per 2.5° grid box for 1950–2009. Blue rectangles denote regions used to define the ∇SST_{EQ} index. White contours indicate SST anomalies regressed onto the ATL3 index. **b**, The June–August ∇SST_{EQ} index with error bars (shade; see Methods). Warm (cold) Atlantic Niño events are marked with filled (open) triangles. The red line indicates the linear regression of ∇SST_{EQ}. **c**, The 21-year running r.m.s. variances of June–August ∇SST_{EQ} (black) and Guinea coast precipitation (red).

[1]International Pacific Research Center, SOEST, University of Hawaii at Manoa, 1680 East West Road, Honolulu, Hawaii 96822, USA, [2]Department of Meteorology, SOEST, University of Hawaii at Manoa, Honolulu, Hawaii 96822, USA. *e-mail: tokinaga@hawaii.edu.

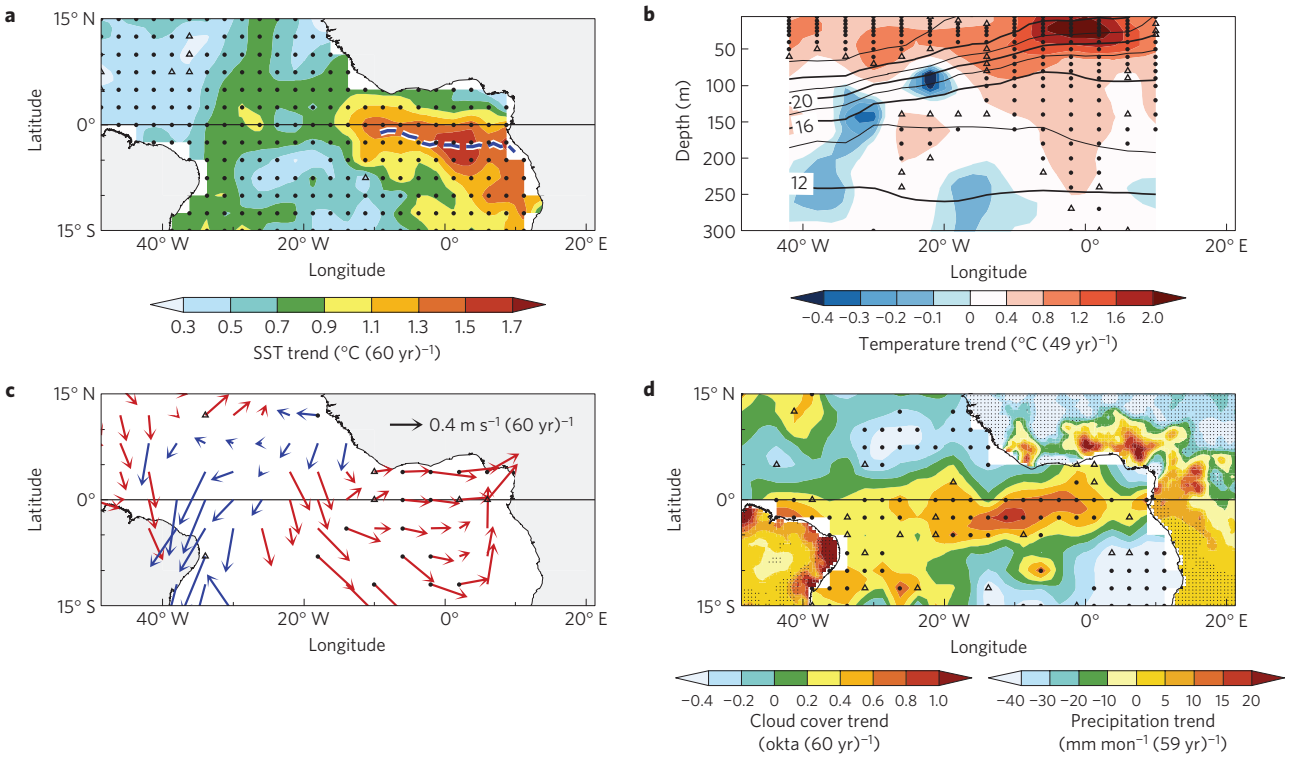

Figure 2 | Patterns of tropical Atlantic climate change. a, June–August SST. The blue dashed line denotes the axis of the climatological equatorial cold tongue. **b**, Longitude–depth section of June–August ocean temperature averaged over 4° S–4° N. The climatology is shown by contours at 1 °C intervals. **c**, May–July surface wind. Westerly (easterly) trends are shown by red (blue) arrows. **d**, June–August marine cloud cover and land precipitation. Grid points marked with filled circles (triangles) exceed the 95% (90%) confidence level based on the Mann-Kendall[25] test.

with frequent observations of surface meteorologies in the region (Fig. 1a). For 1950–2009, monthly mean SSTs on a 2.5° grid are available for more than 99% of the total months along these ship tracks. To represent zonal gradient change amid a broad warming, we define an equatorial zonal SST difference index (∇SST_{EQ}) for June–August between two main ship lanes in the eastern and western equatorial Atlantic (Fig. 1b). A significant upward trend in ∇SST_{EQ} is apparent since the 1950s, representing a weakening of the equatorial cold tongue. The Sen trend slope[13] for ∇SST_{EQ} is $+0.66 \pm 0.52\,(0.44)$ °C per 60 years at $p = 0.05\,(0.1)$, which corresponds to a $25 \pm 20\,(17)$% reduction of the climatological zonal SST gradient on the equator. Associated with this mean state change, interannual variability of ∇SST_{EQ} has decreased by $48 \pm 13\,(11)$% at $p = 0.05\,(0.1)$ in root-mean-square (r.m.s.) variance for 1960–1999 (Fig. 1c), indicating a significant weakening of the Atlantic Niño mode. The result holds for SST averaged over the Atlantic3 (ATL3) region[14], an index often used for the Atlantic Niño. ∇SST_{EQ} correlates highly with ATL3 SST ($r = +0.93$). It captures 78% of events with ATL3 SST exceeding 0.5 standard deviation, including major events in 1963, 1968, 1984 and 1991. Remarkably, the r.m.s. variance of Guinea coast precipitation has concurrently decreased by $44 \pm 10\,(8)$% at $p = 0.05\,(0.1)$ for 1960–1998.

The weakening of the equatorial Atlantic cold tongue is conspicuous in the spatial distribution of the June–August SST trend (Fig. 2a). Whereas SST has warmed over the whole domain, a warm-tongue pattern resembling the Atlantic Niño emerges. The local warming maximum is located just along the climatological axis of the equatorial cold tongue, exceeding $1.5 \pm 0.6\,(0.45)$ °C at $p = 0.05\,(0.1)$ in magnitude for the past six decades. A similar tongue-like warming pattern is found in other *in situ* SST and night-time marine-air temperature products (Supplementary Figs S1,S2). Expendable bathythermograph (XBT) observations show a strong subsurface warming up to 250 m depth in the east (Fig. 2b), representing a deepened thermocline. The resultant weakening of subsurface feedback on SST is consistent with the reduced Atlantic Niño variability (Fig. 1c), as corroborated by a mixed-layer heat budget analysis (Supplementary Figs S3–S5).

Surface winds are an important element of tropical ocean–atmosphere interaction, but ship-based wind measurements suffer from a spurious upward trend because of the recent increase in ship size and anemometer height. We have developed a new surface wind product with the innovative use of wind–wave height observations to remove the artificial wind speed trend[15]. Analysis of this new data set reveals that the warm-tongue SST trend is coupled with a long-term relaxation of the equatorial trade winds east of 25° W (Fig. 2c), whereas the uncorrected data show a spurious intensification of the prevailing southeasterlies. The relaxed trade winds suppress equatorial upwelling, leading to a deepened thermocline and intensified SST warming in the eastern equatorial Atlantic. Net surface heat flux shows a trend to cool the ocean owing to the evaporative damping of increased SST and a decrease in solar radiation (Supplementary Fig. S2b), supporting the result that ocean dynamical adjustments cause the warm-tongue SST trend. The ocean GCM forced by our surface wind product successfully reproduces the equatorial Atlantic cold tongue and its observed changes (Supplementary Figs S3–S5). Consistent with the observed deepening of the thermocline, the ocean GCM hindcast illustrates that the weakened vertical entrainment of cold water is a main factor for the weakened cold tongue in the mean and reduced Atlantic Niño variability.

Changes in marine cloud cover and land precipitation are also consistent with the intensified SST warming in the eastern equatorial Atlantic (Fig. 2d). A zonal band of increased cloud cover appears with an equatorial maximum on the western edge of the tongue-like SST trend, representing a southward shift of the intertropical convergence zone (ITCZ).

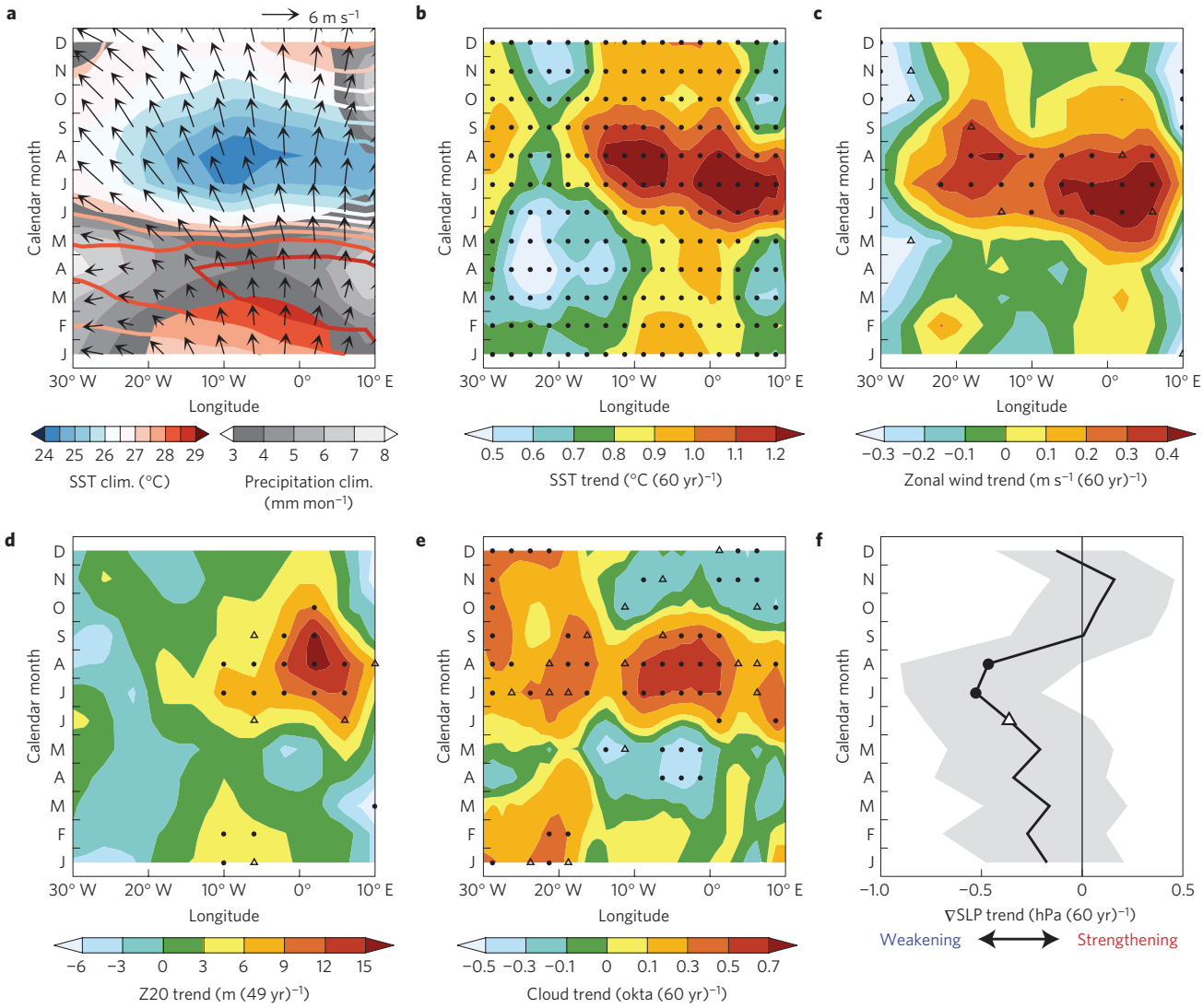

Figure 3 | Weakening of the annual cycles in the equatorial Atlantic. a–e, Longitude–month sections of climatological SST (colour), precipitation (grey) and surface wind vectors (**a**), and trends in SST (**b**), zonal wind (**c**), 20 °C isothermal depth (**d**) and cloud cover (**e**) averaged over 4° S–4° N. **f**, Trend in zonal SLP difference between the eastern (5°–10° W, 8° S–2° N) and central (30°–35° W, 5° S–5° N) equatorial Atlantic (∇SLP). The grey shading indicates 95% confidence intervals based on the Sen median slope method[13]. In **b–f**, grid points marked with filled circles (open triangles) exceed the 95% (90%) confidence level based on the Mann–Kendall[25] test.

Land precipitation has increased (decreased) over the equatorial Amazon, equatorial West Africa and on the Guinea coast (over the Sahel). The precipitation trend on the Guinea coast seems to be insignificant in the June–August mean, but significant for August and September, accompanied by consistent patterns of marine cloud cover (Supplementary Fig. S6). These trend patterns in cloud/precipitation are quite similar to their interannual counterparts during warm Atlantic Niño events[3], indicating that atmospheric convection change is coupled with equatorial Atlantic SST.

Next we examine the seasonality of observed trends. The climatological annual cycle in the equatorial Atlantic is characterized by cold (warm) SSTs, strong (weak) trade winds, and small (large) precipitation in boreal summer (spring; Fig. 3a). The observed SST trend exhibits a maximal (minimal) warming in July (March) when the mean ocean upwelling is enhanced (suppressed; Fig. 3b). This represents a 10–20% reduction of the climatological annual cycle. The equatorial westerly trend also peaks in June–August (Fig. 3c), consistent with a reduction in equatorial zonal sea level pressure gradient (∇SLP) that peaks in June–August (Fig. 3f). In response to the equatorial westerly trend, the 20 °C isothermal depth (Z20), representative of the thermocline depth, shows a maximal deepening in July–September (~10–15 m for the past five decades) (Fig. 3d) when the climatological thermocline shoals. The amplitude of the Z20 annual cycle in the eastern equatorial Atlantic has decreased by 40–60% relative to the climatology, more than three times larger than the weakening of the SST annual cycle in percentage. The trend of increased cloud cover also peaks in July–August (Fig. 3e). The common seasonality of the observed trends represents a significant weakening of the annual cycle in equatorial Atlantic climate, giving us confidence in the results.

What external forcing causes the weakened equatorial Atlantic cold tongue? The Atlantic meridional overturning circulation (AMOC) may affect the tropical Atlantic, as in the Younger Dryas and Heinrich events[16]. SST warming (cooling) in the tropical South (North) Atlantic is a robust response among water-hosing experiments that shut down AMOC. This weakened interhemispheric SST gradient acts to relax cross-equatorial southeasterlies, thereby reducing equatorial upwelling. However, the role of AMOC is unclear in recent observed changes over

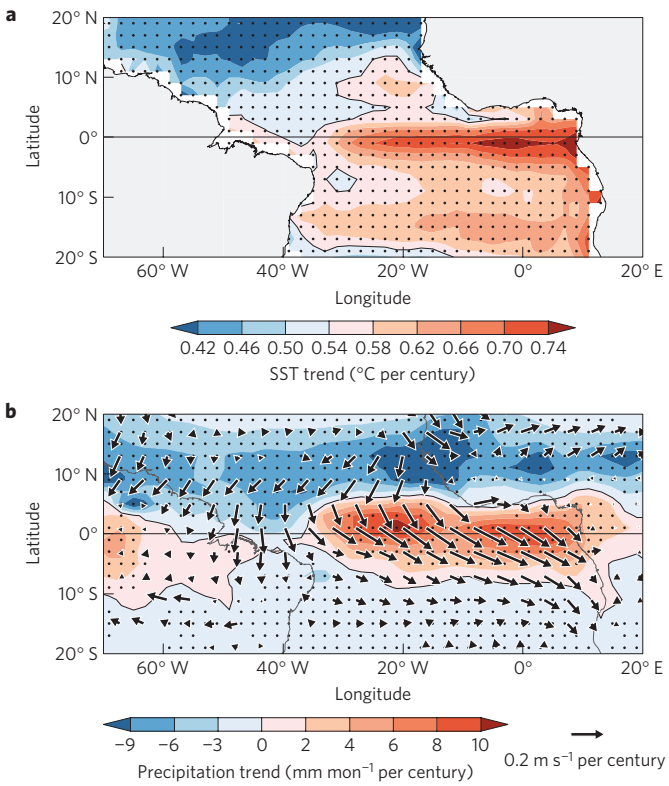

Figure 4 | Patterns of the simulated climate change for 1900–1999. **a**,**b**, SST (colour) (**a**), surface wind (vector) and precipitation (colour) (**b**) for June–August, based on the ensemble mean of the climate of the twentieth-century experiments from 19 CMIP3 models. For SST and precipitation trends, grid points marked with filled circles exceed the 95% confidence level based on the Mann–Kendall[25] test. For surface wind trend, only vectors exceeding the 95% confidence level are plotted.

the equatorial Atlantic for the following reasons. First, it remains unclear whether AMOC has weakened for recent decades[17,18]. Second, the Atlantic multidecadal oscillation[19], linked to AMOC variability, has no significant correlation with ∇SST_{EQ} variability over the past century (Supplementary Fig. S7 and Table S1).

The anthropogenic aerosol-cooling effect, stronger in the Northern than in the Southern Hemisphere, could cause hemispheric asymmetry in SST warming[20]. CMIP3 twentieth-century experiments with sulphate aerosol forcing tend to feature a weakening meridional SST gradient and the relaxed southeasterlies across the Atlantic equator (Fig. 4). Interestingly, the centennial trend in interhemispheric SST gradient significantly correlates with that in ∇SST_{EQ} among models ($r = -0.7$; Supplementary Fig. S8). The multi-model ensemble exhibits a weakening of zonal SST gradient with a maximal SST warming in the eastern equatorial Atlantic (Fig. 4a) and a reduced seasonal cycle (Supplementary Fig. S9). This SST warming pattern anchors a zonal band of increased precipitation over the equatorial Atlantic that extends to the Amazon and West Africa (Fig. 4b), bearing a striking resemblance to our cloud/precipitation observations. The patterns of simulated climate change indicate a strong coupling between the zonal and meridional gradients of equatorial SST through the cross-equatorial trade winds, a coupling previously seen in the seasonal cycle[21]. The reduction in both zonal and meridional SST gradients forces the ITCZ southward, contributing to the drying trend observed over the Sahel[22]. Consistent with our hypothesis, recent coupled GCM experiments showed that anthropogenic aerosols induce a southward shift of the ITCZ and weaken the meridional SST gradient for the twentieth century[23]. CMIP3 models simulate too weak a cold tongue[5]. It remains to be determined to what extent such model biases alter the simulation of climate change patterns.

Our observational study reveals robust changes in the equatorial Atlantic over the past six decades, most notably a locally enhanced SST warming in the east, weakened trade winds, deepened thermocline and enhanced atmospheric convection. These changes are characteristic of Bjerknes feedback[24], a mechanism key to the development of interannual Atlantic Niño events. These changes in the equatorial Atlantic are most pronounced in boreal summer, representing a marked decrease in seasonal cycle. Remarkably, the Atlantic Niño weakens substantially in interannual variance of SST and precipitation. The ocean GCM hindcast supports our hypothesis that suppressed thermocline feedback plays a primary role in reducing SST variability in both space and time over the equatorial Atlantic.

Although the rise of global mean temperature may have been dominated by increased greenhouse gas (GHG) concentrations, our results indicate that other climate forcing can be important for regional patterns of observed climate changes over the tropical Atlantic. Model projections under the GHG emission scenario A1B indicate a broad SST warming without an obvious change in cross-equatorial SST gradient in the tropical Atlantic, deviating markedly from their simulations for the twentieth century (Supplementary Fig. S10 versus Fig. S4)[23]. If aerosol cooling is the main cause of recent equatorial Atlantic change as described in this study, the tropical Atlantic may experience yet another major shift given that the GHG increase is likely to dominate over aerosol effects in coming decades. Such a shift in patterns of climate change (that is, precipitation, sea level and oceanic nutrients) has important impacts on the socio-economy of regions surrounding the tropical Atlantic. If Atlantic Niño variability is to recover in the future, the resultant increase in climate extremes would add burdens to an ecosystem and society already under the stress of global warming.

Methods

Estimate of long-term trends. All trends were calculated using only well-sampled grid boxes that contain monthly means for more than 70% of the total months, to reduce sampling errors. To suppress subseasonal variabilities, all monthly mean data were smoothed with a three-month running average before the trend analysis. We estimated long-term trends and their statistical significance with the Sen median slope[13] and the Mann–Kendall[25] test, respectively, both of which are non-parametric methods less affected by outliers sometimes contained in observations. If the linear trend and Student's t-test are applied for the same data, our conclusions do not change. The analysis period is from 1950 to 2009, except for subsurface temperature, which starts in the 1960s, and land precipitation, which ends in 2008. For visualization, we applied a weighted average using values at the grid point and eight surrounding points.

International Comprehensive Ocean–Atmosphere Data Set. Ship-observed SST, SLP and marine cloud cover were used from the International Comprehensive Ocean–Atmosphere Data Set (ICOADS) release 2.5 (ref. 26) to construct a 2.5° longitude–latitude gridded monthly mean data set. All data have been trimmed using a quality control that identifies potential outliers based on the climatological 3.5 standard-deviation limits. This is basically the same quality control as used for the standard product of the ICOADS Monthly Summary Groups available at the Research Data Archive at the National Center for Atmospheric Research. Ship-observed marine cloud cover is known to have systematic bias[27]. To eliminate the bias, we removed the tropical (30° N–30° S) mean cloud cover trend from each oceanic grid box[28]. We defined the ∇SST_{EQ} index as the zonal difference in SST anomaly between (20° W–0°, 3° S–3° N) and (25°–45° W, 3° S–3° N) (blue rectangles in Fig. 1a), using only well-sampled grid boxes with monthly means for more than 99% of the total months. Error bars in Fig. 1b are defined as yearly standard deviation of June–August SSTs averaged in the two rectangles. The ATL3 SST index was defined as the SST anomaly averaged over 20° W–0°, 3° S–3° N (ref. 14). All original data are available from the Research Data Archive at the National Center for Atmospheric Research.

EN3 XBT. Ocean subsurface temperatures are obtained from XBT profiles in the Enhanced Ocean Data Assimilation and Climate Prediction archive version 3 (EN3) available at the Met Office Hadley Centre. XBTs were developed in the early 1960s, but are known to have a time-varying warm bias due to changes in the fall rate of their probes. We analysed only bias-corrected XBT profiles in EN3 (ref. 29), and constructed a 4° longitude–latitude gridded monthly mean data set of subsurface

temperature for 1961–2009. All temperature profiles have been trimmed using basically the same quality control as used for ICOADS.

Wave- and Anemometer-based Sea-surface Wind. We used sea surface winds from the Wave- and Anemometer-based Sea-surface Wind (WASWind) data set available on a 4° grid for 1950–2009 (ref. 15). This data set was constructed from ship-observed winds and wind-wave heights in ICOADS. It is well known that the ship-observed surface winds have a spurious upward trend due to the increase in anemometer height, making it difficult to identify long-term changes in marine surface wind. The WASWind product substantially reduces such spurious trends by a stability-dependent height correction for measured winds and using wind-wave height to estimate surface wind speed. Not only does this surface wind product successfully reproduce major modes of seasonal-to-decadal variability, but its trend patterns are also in good agreement with SLP measurements and satellite measurements for the recent decades. All this illustrates the utility of WASWind for climate trend analysis.

Precipitation. For land precipitation, we used a 0.5° longitude–latitude gridded monthly mean data set available from the University of Delaware. This precipitation data set was constructed from rain gauge observations with climatologically aided interpolation[30]. The time series of Guinea coast precipitation in Fig. 1c is based on the average over 2°–10° E, 4°–8° N, where land precipitation anomalies significantly correlate with the Atlantic Niño. For climatological precipitation over the ocean, the Global Precipitation Climatology Project (GPCP) data set was used for 1979–2008.

CMIP3 models. We analysed the 'Climate of the twentieth century experiments' from 19 coupled GCMs participating in CMIP3 (see Supplementary Information). The 19 coupled GCMs were forced by GHGs and sulphate aerosol effects during the twentieth century, providing surface wind, SST and precipitation. We produced a multi-model ensemble mean by averaging results from the 19 coupled GCMs, and estimated its centennial June–August trend for 1900–1999.

Received 23 September 2010; accepted 7 January 2011; published online 6 February 2011

References

1. Carton, J. A., Cao, X. H., Giese, B. S. & daSilva, A. M. Decadal and interannual SST variability in the tropical Atlantic Ocean. *J. Phys. Oceanogr.* **26,** 1165–1175 (1996).
2. Hirst, A. C. & Hastenrath, S. Atmosphere–ocean mechanisms of climate anomalies in the Angola-tropical Atlantic sector. *J. Phys. Oceanogr.* **13,** 1146–1157 (1983).
3. Ruiz-Barradas, A., Carton, J. A. & Nigam, S. Structure of interannual-to-decadal climate variability in the tropical Atlantic sector. *J. Clim.* **13,** 3285–3297 (2000).
4. Boyd, A. J., Tauntonclark, J. & Oberholster, G. P. J. Spatial features of the near-surface and midwater circulation patterns off western and southern South Africa and their role in the life histories of various commercially fished species. *S. Afr. J. Mar. Sci.* **12,** 189–206 (1992).
5. Richter, I. & Xie, S-P. On the origin of equatorial Atlantic biases in coupled general circulation models. *Clim. Dyn.* **31,** 587–598 (2008).
6. Xie, S-P. *et al.* Global warming pattern formation: Sea surface temperature and rainfall. *J. Clim.* **23,** 966–986 (2010).
7. Clement, A. C., Baker, A. C. & Leloup, J. Climate change: Patterns of tropical warming. *Nature Geosci.* **3,** 8–9 (2010).
8. Vecchi, G. A. *et al.* Weakening of tropical Pacific atmospheric circulation due to anthropogenic forcing. *Nature* **441,** 73–76 (2006).
9. Vecchi, G. A., Clement, A. & Soden, B. J. Examining the tropical Pacific's response to global warming. *Eos Trans. AGU* **89,** 81 (2008).
10. Han, W. *et al.* Patterns of Indian Ocean sea-level change in a warming climate. *Nature Geosci.* **3,** 509–584 (2010).
11. Zheng, X. T., Xie, S-P., Vecchi, G. A., Liu, Q. Y. & Hafner, J. Indian Ocean dipole response to global warming: Analysis of ocean-atmospheric feedbacks in a coupled model. *J. Clim.* **23,** 1240–1253 (2010).
12. Abram, N. J., Gagan, M. K., Cole, J. E., Hantoro, W. S. & Mudelsee, M. Recent intensification of tropical climate variability in the Indian Ocean. *Nature Geosci.* **1,** 849–853 (2008).
13. Sen, P. K. Estimates of the regression coefficient based on Kendall's tau. *J. Am. Stat. Assoc.* **63,** 1379–1389 (1968).
14. Zebiak, S. E. Air–sea interaction in the equatorial Atlantic region. *J. Clim.* **6,** 1567–1568 (1993).
15. Tokinaga, H. & Xie, S-P. Wave- and Anemometer-based Sea-surface Wind (WASWind) for climate change analysis. *J. Clim.* **24,** 267–285 (2011).
16. Chang, P. *et al.* Oceanic link between abrupt changes in the North Atlantic Ocean and the African monsoon. *Nature Geosci.* **1,** 444–448 (2008).
17. Bryden, H. L., Longworth, H. R. & Cunningham, S. A. Slowing of the Atlantic meridional overturning circulation at 25° N. *Nature* **438,** 655–657 (2005).
18. Wang, C. Z., Dong, S. F. & Munoz, E. Seawater density variations in the North Atlantic and the Atlantic meridional overturning circulation. *Clim. Dyn.* **34,** 953–968 (2010).
19. Enfield, D. B., Mestas-Nunez, A. M. & Trimble, P. J. The Atlantic multidecadal oscillation and its relation to rainfall and river flows in the continental US. *Geophys. Res. Lett.* **28,** 2077–2080 (2001).
20. Chang, C-Y. *et al.* Sulfate aerosol control of tropical Atlantic climate over the 20th century. *J. Clim.* doi:10.1175/2010JCLI4065.1 (2011, in the press).
21. Philander, S. G. H. & Pacanowski, R. C. A model of the seasonal cycle in the tropical Atlantic Ocean. *J. Geophys. Res.* **91,** 14192–14206 (1986).
22. Giannini, A., Saravanan, R. & Chang, P. Oceanic forcing of Sahel rainfall on interannual to interdecadal time scales. *Science* **302,** 1027–1030 (2003).
23. Kawase, H. *et al.* Physical mechanism of long-term drying trend over tropical North Africa. *Geophys. Res. Lett.* **37,** L09706 (2010).
24. Bjerknes, J. Atmospheric teleconnections from the equatorial Pacific. *Mon. Weath. Rev.* **97,** 163–172 (1969).
25. Kendall, M. G. *Rank Correlation Methods* (Griffin, 1975).
26. Woodruff, S. D. *et al.* ICOADS Release 2.5: Extensions and enhancements to the surface marine meteorological archive. *Int. J. Climatol.* doi:10.1002/joc.2103 (2010).
27. Norris, J. R. Trends in upper-level cloud cover and surface divergence over the tropical Indo-Pacific Ocean between 1952 and 1997. *J. Geophys. Res.* **110,** D21110 (2005).
28. Deser, C. & Phillips, A. S. Simulation of the 1976/77 climate transition over the North Pacific: Sensitivity to tropical forcing. *J. Clim.* **19,** 6170–6180 (2006).
29. Wijffels, S. E. *et al.* Changing expendable bathythermograph fall rates and their impact on estimates of thermosteric sea level rise. *J. Clim.* **21,** 5657–5672 (2008).
30. Willmott, C. J. & Robeson, S. M. Climatologically aided interpolation (CAI) of terrestrial air temperature. *Int. J. Climatol.* **15,** 221–229 (1995).

Acknowledgements

The work was supported by NOAA, NSF, NASA and JAMSTEC. We thank T. Ogata for conducting the ocean GCM hindcast.

Author contributions

H.T. and S-P.X. contributed to the central ideas presented in the paper. H.T. compiled and analysed ship observations. H.T. and S-P.X. wrote the paper.

Additional information

The authors declare no competing financial interests. Supplementary information accompanies this paper on www.nature.com/naturegeoscience. Reprints and permissions information is available online at http://npg.nature.com/reprintsandpermissions. Correspondence and requests for materials should be addressed to H.T.